The structure of decagonal $Al_{70.5}Mn_{16.5}Pd_{13}$

1994 J. Phys.: Condens. Matter 6 613

(http://iopscience.iop.org/0953-8984/6/3/004)

J. Phys.: Condens. Matter 6 (1994) 613–632. Printed in the UK

The structure of decagonal $Al_{70.5}Mn_{16.5}Pd_{13}$

W Steurer†, T Haibach†, B Zhang†, C Beeli‡ and H-U Nissen‡

† Institut für Mineralogie der Universität Hannover, Welfengarten 1, D-30167 Hannover, Federal Republic of Germany

‡ Laboratorium für Festkörperphysik der ETH-Zürich, CH-8093 Zürich, Switzerland

Received 26 July 1993, in final form 18 October 1993

Abstract. The structure of the stable decagonal quasicrystal $Al_{70.5}Mn_{16.5}Pd_{13}$ was determined by single-crystal x-ray methods. Higher-dimensional structure-solution techniques were employed, such as five-dimensional (5D) Patterson and Fourier syntheses as well as 5D least-squares structure refinements. A 3D physical-space maximum-entropy method (MEM) was used in the course of structure-factor phasing and for the calculation of a high-quality electron-density distribution function. Geometrically, the structure may be described as a periodic stacking of two different quasiperiodic layers A (puckered ±0.3 Å) and B (planar) with sequence ABAaba (a and b denote the layers A and B, respectively, rotated by $2\pi/10$), consistent with the centrosymmetric 5D superspace group $P10_5/mmc$. Basic structure-building elements, however, are columnar clusters (⌀ ~ 20 Å) with cross-sections corresponding to parts of a decorated Penrose tiling. The clusters are packed in a way that results in a disordered Robinson-triangle tiling. The title compound is isotypic to metastable decagonal $Al_{78}Mn_{22}$ and locally shows a strong resemblance to icosahedral $Al_{68.7}Mn_{9.6}Pd_{21.7}$, orthorhombic Al_3Mn and hexagonal μ-$Al_{4.12}Mn$.

1. Introduction

Decagonal phases combine the structural characteristics of both quasicrystals and regular crystals: the atoms are quasiperiodically ordered in planes which, by contrast, are stacked with translational periodicity. This picture, however, should only be taken as a geometrical description. A specifically physical description is the interpretation of decagonal phases as quasiperiodically packed columnar clusters, which themselves are periodic along their tenfold screw axes (cf Steurer *et al* 1993, referred to in what follows as the ACN paper). The translation periods of the decagonal phases known so far are ~ 4 Å, ~ 8 Å, ~ 12 Å, ~ 16 Å, ~ 24 Å and ~ 36 Å corresponding to 2-, 4-, 6-, 8-, 12- and 18-layer stackings respectively (Steurer 1990, Okabe *et al* 1992). Decagonal $Al_{70.5}Mn_{16.5}Pd_{13}$ with ~ 12 Å translational periodicity was first found and investigated by high-resolution transmission electron microscopy (HRTEM) by Beeli and co-workers (1991). Further HRTEM studies were performed by Hiraga and co-workers (1991), Hiraga and Sun (1993) and Beeli and Nissen (1993), while single-crystal x-ray studies were reported by Steurer (1993) and Frey and Steurer (1993). Tsai and co-workers (1991) discovered a second stable (?) decagonal phase in the Al–Mn–Pd system with 16 Å translational periodicity and a chemical composition near $Al_{70}Mn_5Pd_{25}$. Since the two binary decagonal phases Al_5Pd, with ~ 16 Å period (Ma *et al* 1988), and $Al_{78}Mn_{22}$, with ~ 12 Å period (Steurer 1991), are metastable, the title compound may be seen as Pd-stabilized $Al_{78}Mn_{22}$ and decagonal $Al_{70}Mn_5Pd_{25}$ as Mn-stabilized Al_5Pd. Thus, decagonal $Al_{70.5}Mn_{16.5}Pd_{13}$ was expected to be isostructural with metastable decagonal $Al_{78}Mn_{22}$. The present work was primarily undertaken to clarify this view.

0953-8984/94/030613+20$07.50

2. Experimental details

An alloy ingot with nominal composition $Al_9Mn_2Pd_2$ was prepared by melting a mixture of Al (99.997%), Mn (99.9%) and Pd (99.9+%) in a plasma jet furnace. Subsequently, the sample was annealed at 810°C for 35 min on Ta foil in a quartz ampulla under Ar (99.999%) atmosphere and with Ti grains as getter material. The ingot was crushed and several crystals with decaprismatic morphology were ground to spheres in a Bond chamber. An approximately spherical crystal with 0.10(2) mm diameter was selected after checking for sharp reflections by Laue photographs. For the characterization of the quality of the single crystals and the exploration of the distribution of Bragg reflections as well as diffuse scattering, numerous x-ray photographs were taken using the Buerger precession technique (figure 1). The photographs were overexposed with regard to the strongest Bragg reflections by about a factor of 100 to make even very weak diffuse scattering and satellite reflections observable. All Bragg reflections on the photographs can be indexed using the basis vectors $\boldsymbol{a}_i^*$, $i = 1, \ldots, 5$ (see section 3). The diffuse scattering is condensed in regions having the shape of outlined pentagons, which are arranged in decagonal rings around strong Bragg reflections. The pentagon corners s nearer to the central Bragg spot m (figure 1(*a*)) may be indexed on the basis of wave vectors $\boldsymbol{a}_i^{s*} = 0.124\boldsymbol{a}_i^*$, $i = 1, \ldots, 4$. The same wave vectors were used for indexing the sharp satellite spots of decagonal $Al_{70}Co_{15}Ni_{15}$ (cf figure 1 of the ACN paper). The stoichiometry of the decagonal phase was determined to be $Al_{70.5}Mn_{16.5}Pd_{13}$ by quantitative x-ray microanalysis on the SEM (Beeli *et al* 1991).

The data collection was performed on an Enraf-Nonius CAD4 four-circle single-crystal diffractometer equipped with graphite monochromator (Mo Kα, $\lambda = 0.7107$ Å) in the $\theta/2\theta$-scan mode. In a first run a unique set of 6647 Bragg reflection intensities was collected within $0 < \theta < 45°$, the indices in the range $-6 < h_i < 6$, $i = 1, \ldots, 4$, $0 < h_5 < 24$ and the length of the 5D diffraction vector $|\boldsymbol{H}| \leqslant 2$ Å^{-1}. All reflections with intensities $I(\boldsymbol{H}) > 2\sigma[I(\boldsymbol{H})]$ were recollected within ten different asymmetric units in order to obtain better counting statistics and to minimize the influence of systematic errors. Thus, additional 11010 intensities were measured and corrected for Lorentz and polarization effects. A spherical absorption correction was performed with minimum and maximum transmission factors 0.128 and 0.181, respectively; the linear absorption coefficient $\mu = 15$ mm^{-1} was calculated from the mass absorption coefficients μ_k/ρ of the elements (*International Tables for X-ray Crystallography* 1974). The corrected intensities were averaged, yielding 476 unique reflections ($R_i = 0.053$) with $I(\boldsymbol{H}) > 3\sigma[I(\boldsymbol{H})]$. Reflections with intensities $I(\boldsymbol{H}) \leqslant 3\sigma[I(\boldsymbol{H})]$ could not be separated adequately from the underlying diffuse background and were rejected. The intensity distribution as a function of the perpendicular versus the parallel component of the 5D diffraction vector $\boldsymbol{H} = (\boldsymbol{H}^{\parallel}, \boldsymbol{H}^{\perp})$ is depicted in figure 2.

3. Structure solution and refinement

3.1. Symmetry and metrics

Higher-dimensional structure-solution techniques were used in the same way as described by Steurer (1990, 1991) for decagonal $Al_{78}Mn_{22}$. Thus, only a few definitions will be repeated: the 5D embedding space $\boldsymbol{V} = (\boldsymbol{V}^{\parallel}, \boldsymbol{V}^{\perp})$ consists of two orthogonal subspaces, the 3D physical (parallel, external) space $\boldsymbol{V}^{\parallel}$ with basis vectors $\boldsymbol{v}_1$, $\boldsymbol{v}_2$, $\boldsymbol{v}_3$ and the 2D perpendicular (complementary, internal) space $\boldsymbol{V}^{\perp}$ with basis vectors $\boldsymbol{v}_4$, $\boldsymbol{v}_5$. All physical space reciprocal lattice vectors $\boldsymbol{H}^{\parallel} = h_1^{\parallel}\boldsymbol{a}_1'^* + h_2^{\parallel}\boldsymbol{a}_2'^* + h_3^{\parallel}\boldsymbol{a}_3'^* = h_1\boldsymbol{a}_1^* + h_2\boldsymbol{a}_2^* + h_3\boldsymbol{a}_3^* + h_4\boldsymbol{a}_4^* + h_5\boldsymbol{a}_5^*$, with $h_1^{\parallel}$, $h_2^{\parallel}$

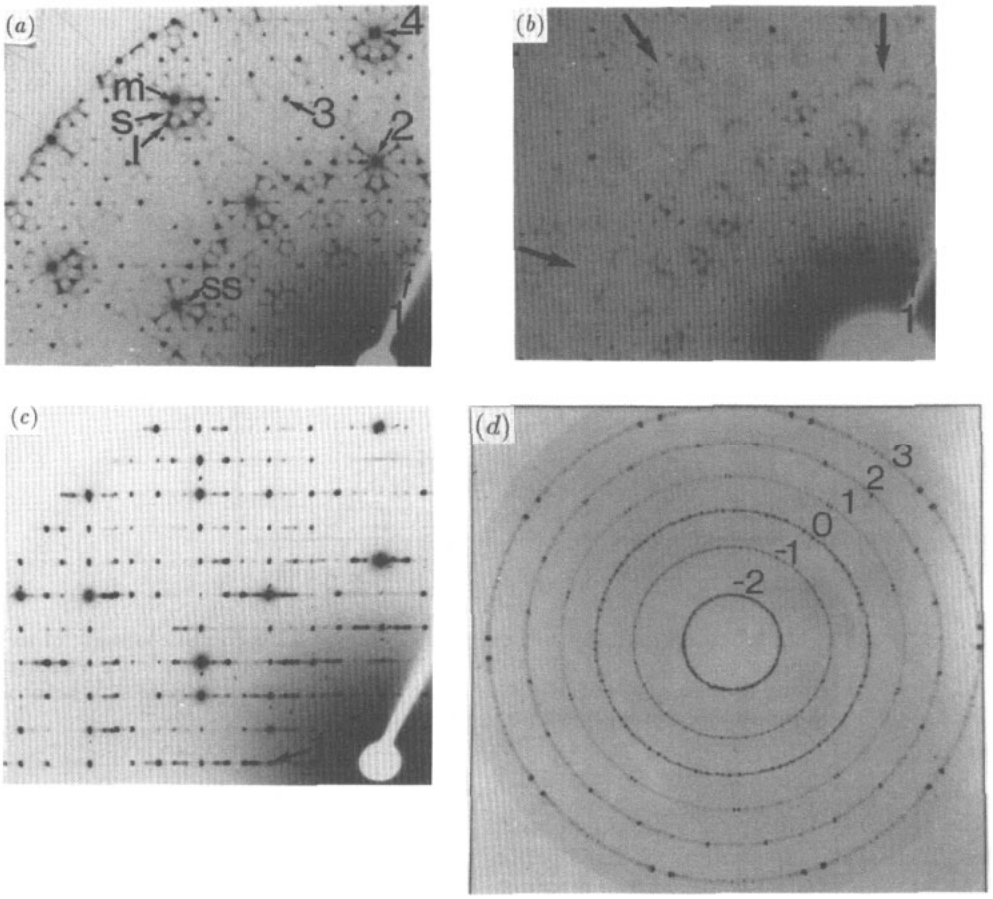

Figure 1. Details of x-ray precession photographs of decagonal $Al_{70.5}Mn_{16.5}Pd_{13}$: (*a*) Zero-layer photograph with the reflections 1(10000), 2(100$\bar{1}$0), 3(110$\bar{1}$0), 4(11$\bar{1}$0) marked. Diffuse pentagons are arranged around strong Bragg reflections m: the inner corners s may be indexed by wave vectors $a_i^{s*} = 0.124a_i^*$, the outer corners 1 by wave vectors $a_i^{1*} = 0.236a_i^*$. There are also satellite reflections ss around strong Bragg reflections, which can be indexed by basis vectors $a_i^{ss*} = 0.124/\tau a_i^* = 0.0766a_i^*$, $i = 1, \ldots, 4$. (*b*) First layer with systematical extinctions between the reciprocal basis vectors, consistent with $10/mmm$ diffraction symmetry. Extinct reciprocal lattice rows are marked by arrows, the (10001) reflection by 1. (*c*) Zero-layer photograph perpendicular to that shown in (*a*) with the (10000) reflection indicated by 1. (*d*) Cone-axis photograph showing very sharp unsplit Bragg spots superposed on diffuse rings (rings are numbered). (Mo Kα, Johansson-type focusing quartz monochromator, Rigaku RU 200 rotating-anode assembly, 0.3 × 0.3 mm^2 fine focus, 60 kV, 90 mA, $\mu = 30°$; 100 mm crystal-to-film distance and ~ 170 h exposure time for (*a*), (*b*) and (*c*); 30 mm distance and 1.5 h for (*d*)).

irrational and $h_3^{\parallel}$, h_i, $i = 1, \ldots, 5$, integer numbers, can be written as linear combinations of the five reciprocal basis vectors $a_i^* = a_i^*(\cos 2\pi i/5, \sin 2\pi i/5, 0)$ with $a_i^* = 0.2570(1)$ Å^{-1}, $i = 1, \ldots, 4$, and $a_5^* = a_5^*(0, 0, 1)$, with $a_5^* = 0.07964(2)$ Å^{-1}. The star of these five reciprocal basis vectors corresponds to a projection of the hypothetical 5D reciprocal basis vectors $d_i^* = (a_i^*, 0, a_{3i}^*)$, $i = 1, \ldots, 4$, $d_5^* = (0, a_5^*, 0)$ onto $V^{\parallel}$. The direct basis vectors (in the following called the d basis), spanning the unit cell in 5D space, can be written in the

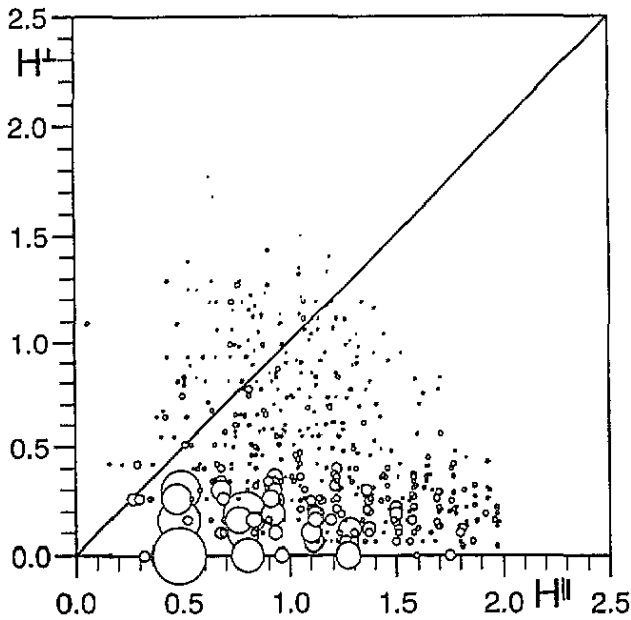

Figure 2. Intensity statistics with the perpendicular versus the parallel component of the diffraction vector $H = (H^{\parallel}, H^{\perp})$. The radius of the circles is proportional to the respective structure amplitudes; the lengths of the diffraction vector components are given in Å^{-1}. For a comparison with Q statistics multiply by a factor of 2π.

form $d_i = 2/(5a_i^*)(\cos 2\pi i/5 - 1, \sin 2\pi i/5, 0, \cos 6\pi i/5 - 1, \sin 6\pi i/5)$, $i = 1, \ldots, 4$, and $d_5 = 1/a_5^*(0, 0, 1, 0, 0)$; the vector components refer to the above-mentioned 5D orthogonal coordinate system spanned by the basis vectors v_i, $i = 1, \ldots, 5$ (in what follows called the v basis). The absolute values of the vectors d_i^*, d_i amount to $d_i^* = 2^{1/2}a_i^* = 0.3635(1)$ Å^{-1}, $i = 1, \ldots, 4$, $d_5^* = a_5^* = 0.07964(2)$ Å^{-1}, and $d_i = 2/(5^{1/2}a_i^*) = 3.480(1)$ Å, $i = 1, \ldots, 4$, $d_5 = 1/a_5^* = 12.557(1)$ Å, respectively; the angles are $\alpha_{ij} = 60°$, $\alpha_{i5} = 90°$, $i, j = 1, \ldots, 4$, and the volume is $V = 5^{1/2}d_i^4 d_5/4 = 1029.8(1)$ Å^5. The 5D least-squares structure refinements were performed on the d basis, the 3D MEM calculations and the graphical representation of the (electron) density maps on the v basis.

For our sample of $Al_{70.5}Mn_{16.5}Pd_{13}$, systematically absent Bragg reflections and diffuse scattering (marked by arrows in figure 1(*b*)) of the type

$$h_1h_2\overline{h_2}\overline{h_1}h_5 : h_5 = 2n + 1 \qquad (0000h_5 : h_5 = 2n + 1)$$

were observed, indicating c-glide planes and a 10_5 screw axis, consistent with 5D superspace groups $P10_5mc$ and $P10_5/mmc$, respectively (Rabson *et al* 1991). $P10_5/mmc$ was used in the course of structure determination since there was no hint for absence of centrosymmetry. The appearance of systematic extinctions in accordance with diffraction symmetry $10/mmm$ is proof that the sample is not simply a five- or tenfold incoherently twinned crystalline material, since the superposition of the diffraction patterns of such twin individuals could never produce systematic absences of the observed symmetry (cf the ACN paper). Because of this fact and since all observable Bragg reflections can be indexed in a way consistent with the 5D reciprocal basis mentioned above, the sample must have at least an average structure that can be described within the nD approach, which is invariant under the operations of

the 5D symmetry group $P10_5/mmc$. From this it does not necessarily follow, however, that the structure has to be quasiperiodic in the strict sense; it may also correspond to a random tiling (Henley 1991) in the broadest sense of the word (including nanocrystalline domains), being quasiperiodic only on average.

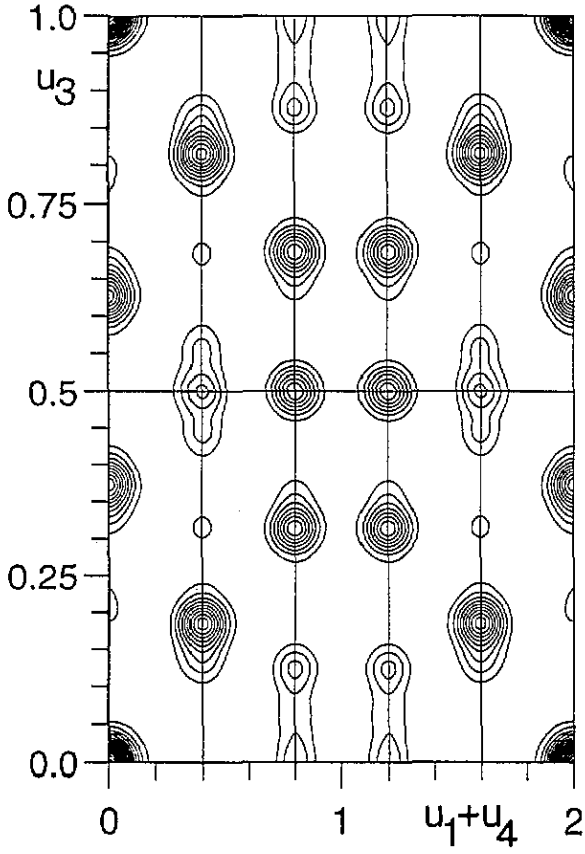

Figure 3. Characteristic (10110) section of the 5D Patterson function. All maxima of one 5D unit cell are located on this special plane. All coordinates are given on the v basis.

3.2. Structure solution

Since the characteristic sections of the respective 5D Patterson functions of decagonal $Al_{70.5}Mn_{16.5}Pd_{13}$ (figure 3) and $Al_{78}Mn_{22}$ (figure 2 of Steurer 1991) proved to be very similar, the 5D structure model proposed for decagonal $Al_{78}Mn_{22}$ was taken as the starting model for the least-squares refinements. With some modifications indicated by 5D difference-Fourier syntheses and MEM density maps a model consisting of four hyperatoms was derived, converging to the final values $R = 0.249$ and $wR = 0.214$ for 33 refined parameters and 476 reflections. In addition to the parameters listed in table 1, some scale factor and one isotropic empirical extinction factor were refined. The quality of the least-squares fit is illustrated in an $F_o(H)/F_c(H)$ plot (figure 4). The R factors are rather high compared to those obtained for the recent structure refinements of the approximant phases: $R = 0.139$, $wR = 0.072$

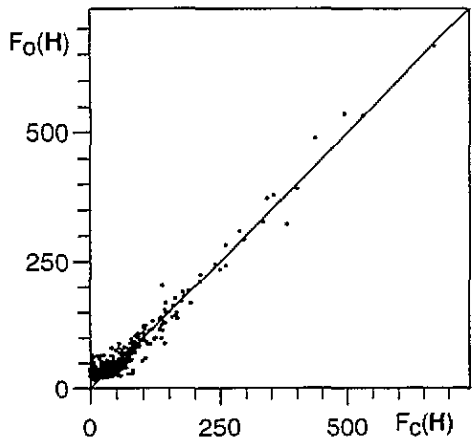

Figure 4. $F_o(H)/F_c(H)$ plot of the final model.

Table 1. Parameters of the refined 5D hyperatoms of decagonal $Al_{70.5}Mn_{16.5}Pd_{13}$: fractional hyperatomic coordinates x_i, $i = 1, \ldots, 5$ (d basis); parallel space temperature factors $B_{11}^{\parallel}$ isotropic in the quasiperiodic layers, and $B_{33}^{\parallel}$ perpendicular to them (Å^2); total site occupancy factor p_k, partial site occupancy factors p_{Al} and p_{Mn}, p_{Pd}; radial hyperatomic size parameter λ_k as a fraction of a_i (a negative value denotes an opposite direction of $\lambda_k e_i$). In the cases with composite hyperatoms, consisting of a small and a large pentagon that are independent of each other or in a pentagram size relation, the parameters of the components are given on successive lines.

Hyperatom	1	2	4	5
Component(s)	two pentagons	pentagram	one pentagon	pentagram
Site symmetry	$5m$	$5m$	$\bar{1}0m2$	$\bar{1}0m2$
Multiplicity	4	4	2	2
x_i, $i = 1, \ldots, 4$	$\frac{1}{5}$	$\frac{3}{5}$	0	$\frac{2}{5}$
x_5	0.0631(3)	0.114(2)	$\frac{1}{4}$	$\frac{1}{4}$
$B_{11}^{\parallel}$	0.3(2)	3(1)	3.6(7)	0.8(6)
	5.3(6)	1.0(6)	—	2.5(5)
$B_{33}^{\parallel}$	0.6(2)	6(2)	7(2)	1.4(9)
	2.5(5)	8(2)	—	0.3(3)
p_k	1	1	1	1
	0.80(8)	*0.53(7)*	—	*0.61(6)*
p_{Al}	0	0.5(2)	1	0
	0.79(6)	0.9(2)	—	0
p_{Mn}	0	0.5(2)	0	0.60(9)
	0.09(5)	0.1(2)	—	0.69(4)
p_{Pd}	*1*	*0*	*0*	*0.40*
	0.12	0	—	0.31
Radius, λ_k	0.147(6)	−0.18	0.39(2)	0.15
	0.45(1)	−0.47(2)	—	0.38(1)

for μ-$Al_{4.12}$ (Shoemaker *et al* 1989), and $R = 0.066$ for Al_3Mn (Hiraga *et al* 1993). This is caused by deficiencies of the refined model but also by experimental problems: as mentioned by Hiraga and co-workers (1991), a single annealed sample may contain regions with perfect decagonal structure besides ones with nanocrystalline or random tiling-like atomic arrangements. In such a case, the Bragg intensities of these structurally different

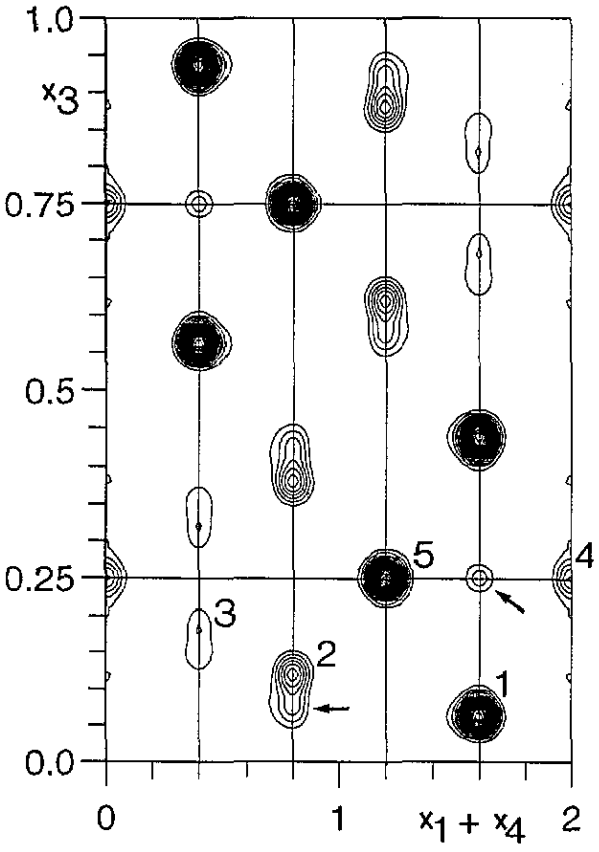

Figure 5. (10110) section of the 5D Fourier function calculated after the last refinement cycle using $F_o(H)$ for Fourier coefficients. The hyperatoms in the asymmetric unit are marked by 1, 2, 3, 4 and 5. The lower part of hyperatom 2 and one other peak (both marked by arrows) are artefacts generated by series truncation effects. All coordinates are given on the v basis.

parts would be superposed coherently and/or incoherently and bias the calculated structure amplitudes. These problems are well known from the structure analysis of regular crystals with microdomain structures. Another experimental problem not satisfactorily solved was the separation of weak Bragg reflections from the structured diffuse background. It has to be pointed out, however, that to date our data set represents the largest data set included successfully in quasicrystal structure refinement. The refined hyperatomic parameters are listed in table 1; the characteristic (10110) Fourier section with refined hyperatoms numbered is plotted in figure 5; figure 6 illustrates (00011) sections of the density distribution of the hyperatoms, with the hyperface fit parameters indicated. The core region of hyperatom 1 corresponds to Pd atoms, the surrounding region mainly to Al. Hyperatom 2 consists of Al/Mn with Mn enriched in its central part, while hyperatom 4 consists of Al only. Hyperatom 5 corresponds to $\sim \frac{1}{3}$ Pd and $\sim \frac{2}{3}$ Mn. Hyperatom 3 was not included in the refinement in order to keep the number of variables low. The low occupation probability of the peripheral regions of the hyperatoms reflects the disordered character of the structure: the atomic surfaces are no longer dense planes in the perpendicular space comparable to the case of fractal structures, for instance. The point density of 0.059 calculated from the

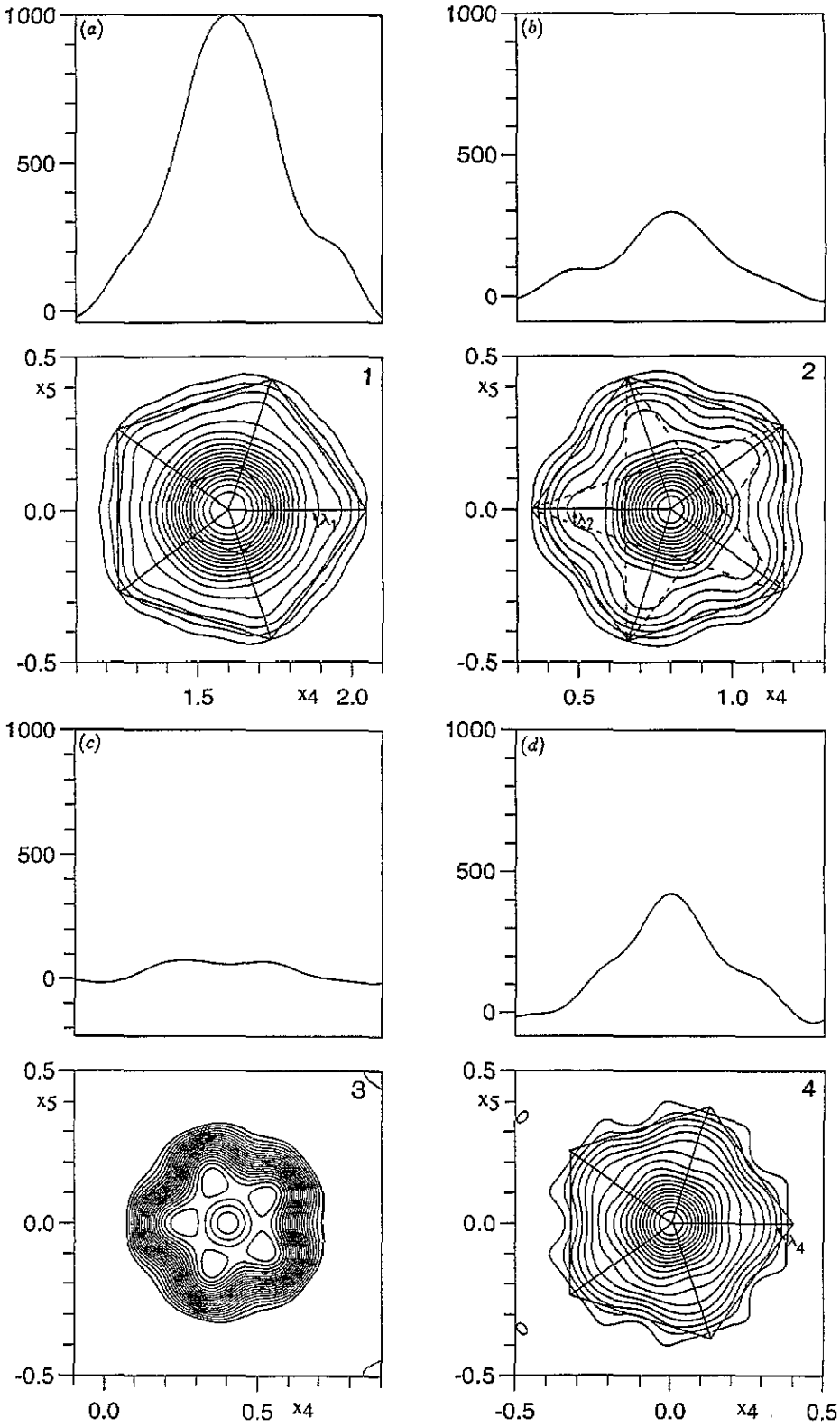
(a)
(b)
(c)
(d)
1000
500
0
1
2
3
4
0.5
x5
0.0
-0.5
1.5
x4
2.0
0.5
1.0
x4
0.0
0.5
x4
-0.5
0.0
x4
0.5
λ1
λ2
λ4

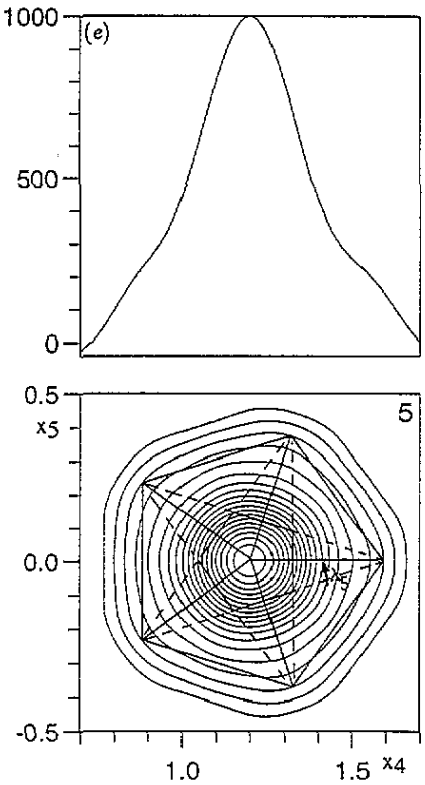

Figure 6. Characteristic perpendicular-space (00011) sections of the 5D Fourier function illustrating the density distribution of (*a*) hyperatom 1 with pentagon parameters λ_k used for parametrization in the refinements. The upper drawing gives the density along $x_5 = 0$. Equivalent sections for the hyperatoms (*b*) 2, (*c*) 3, (*d*) 4 and (*e*) 5. All coordinates are given on the v basis.

least-squares parameters corresponds only to a lower limit as a consequence of the rather crude model refined; the point density estimated from the MEM maps is significantly higher, and that determined from the model is equal to 0.066. For comparison, for icosahedral $Al_{68.7}Mn_{9.6}Pd_{21.7}$ a point density of 0.069 and for the approximant phase Al_3Mn a point of density of 0.068 were derived.

Using solely the Bragg reflections and neglecting the diffuse scattering during the structure analysis is equivalent to averaging over the disordered structure. In terms of the *n*D description, this corresponds to a superposition of hyperatoms of different 5D unit cells that would be identical in an ordered structure but differ from each other in the presence of disorder. A completely satisfying parametrization of the resulting complex hyperatoms would increase the number of variables to be refined in an inadmissible manner. The modelling of the hyperatoms by 5D least-squares refinements was stopped, therefore, after reaching an R factor that was small enough to warrant correct phases (0 or π in our case of a centrosymmetric structure) of at least the larger structure factors. Subsequently, 3D MEM was employed for phasing the remaining structure amplitudes (for a detailed description of this method see the ACN paper): the calculated signs of the 151 largest structure factors ($|F_o(\boldsymbol{H})| \geqslant 0.1|F(000)|$) out of 476 were assigned to the observed structure amplitudes $|F_o(\boldsymbol{H})|$ constituting an MEM starting set. Each MEM calculation was run until $R \leqslant 0.05$

(the expected R factor), then all observed structure amplitudes of the unused set with $(1-x)|F_c(\boldsymbol{H})| \leqslant |F_o(\boldsymbol{H})| \leqslant (1+x)|F_c(\boldsymbol{H})|$, $x = 0.25$ in all cycles but the last one ($x = 0.5$), were supplied with the signs of the respective calculated structure factors and included into the new MEM starting set, and so on. It is emphasized that MEM was applied as a purely 3D technique not affected by any problems of finding a correct 5D basis (5D supercell), since all observable Bragg reflections were self-consistently indexed on a 3D basis. One shortcoming of 3D MEM, however, was the limited size of the 3D electron-density function in the quasiperiodic plane: the MEM calculations were performed on a $1000 \times 1000 \times 80$ grid for a volume of $195 \times 195 \times 12.557$ Å^3 with symmetry taken into account. To transform the 3D structure information into a 5D representation, i.e. to image the 5D hyperatoms, the density obtained by MEM had simply to be lifted (cf the ACN paper).

4. Discussion

4.1. The diffraction pattern

The precession photographs (figure 1) show sharp Bragg reflections, satellites and diffuse scattering condensed in equally sized, outlined pentagons arranged in decagonal rings around strong Bragg reflections. The *sharp* spots on the zero-layer precession photograph give a pattern very similar to that found for the Bragg intensities on an equivalent photograph of decagonal $Al_{70}Co_{15}Ni_{15}$, indicating that the projected average structures (not the real disordered ones!) should be closely related. Indeed, comparing the respective projected electron-density maps (figure 7 of this work and figure 8 of the ACN paper), a similar distribution of large and small wheel-like motifs can be found. These wheels correspond to columnar clusters as known from the structure analysis of decagonal $Al_{70}Co_{15}Ni_{15}$ (cf the ACN paper), and their structures can be reconstructed by evaluating the physical-space sections of the 5D electron-density function (figure 8). Some high-$\boldsymbol{H}^{\perp}$ reflections coincide with outer corners of the diffuse pentagons and might be slightly less sharp than the low-$\boldsymbol{H}^{\perp}$ ones. Shifts of Bragg spots away from their ideal positions indicating anisotropic phason strain are not observed.

The *diffuse* scattering (figure 1) is completely different from that observed for decagonal $Al_{70}Co_{15}Ni_{15}$ (cf figure 1 of the ACN paper). It shows great resemblance to optical diffraction patterns taken from random Robinson-triangle tilings containing nanocrystalline regions (cf figure 3(c) of Welberry 1989) and to electron-diffraction photographs of disordered regions of $Al_{70}Mn_{17}Pd_{13}$, annealed at 800 °C for 4 days (figure 4 of Hiraga *et al* 1991). It has, however, not even the slightest similarity to the diffuse scattering generated by, for instance, random Penrose-rhombus tilings (Welberry 1991).

The intensity ratio of diffuse scattering compared to Bragg scattering, and thereby the amount of disorder present in the structure, can be estimated by means of the cone-axis photograph (figure 1(d)): each ring corresponds to one projected reciprocal lattice layer. *It is found that the intensity of the integrated diffuse scattering is of the same order as* that of the Bragg scattering, as is also found for decagonal $Al_{70}Co_{15}Ni_{15}$ (cf figure 1(f) of the ACN paper). It has to be mentioned that this type of structured diffuse scattering is completely absent in comparable diffraction patterns of decagonal $Al_{78}Mn_{22}$ (cf figure 2 of Steurer and Mayer 1989). Since in our structural study diffuse scattering is neglected, only an average structure can be obtained, which reflects the global properties of decagonal $Al_{70.5}Mn_{16.5}Pd_{13}$. The split positions in the electron density maps (figure 8), as far as they are not caused by series-termination effects, contain the information on all the different orientations and combinations of the clusters that occur in the structure. The atomic

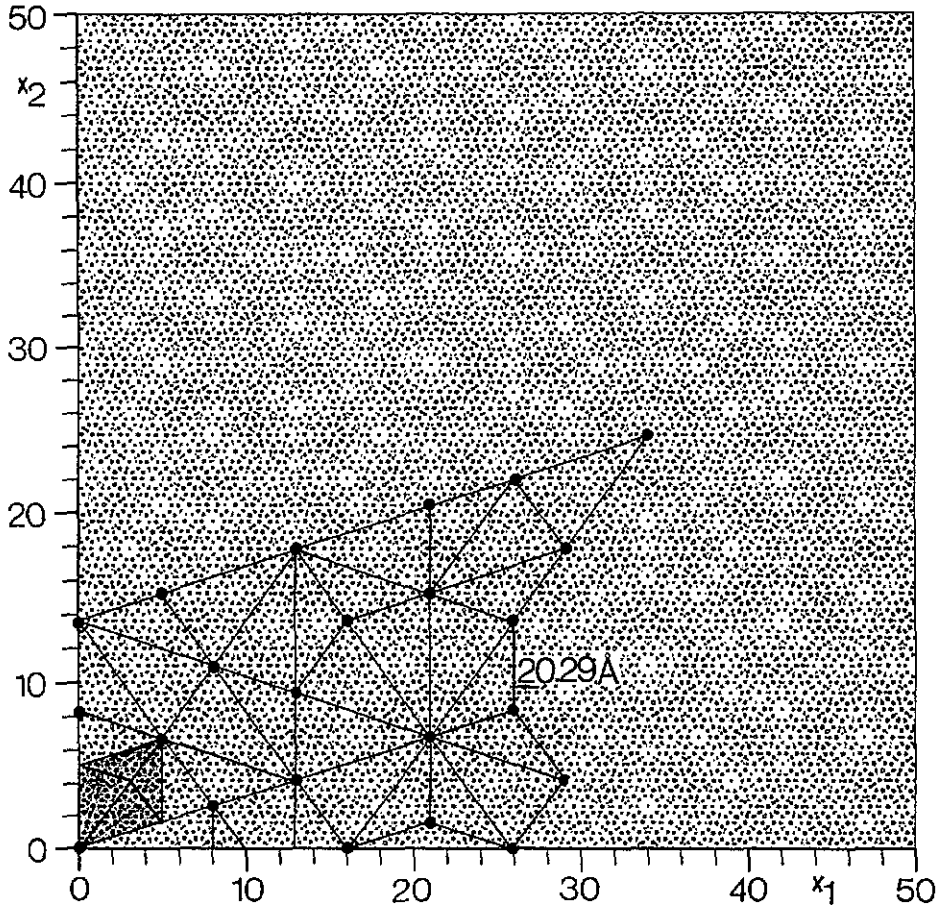

Figure 7. 195 × 195 Å^2 parallel-space (11000) projection of the electron density. One Penrose unit rhombus, with edge length $a_r^s = L = 20.29(1)$ Å and Robinson triangles marked, is shaded. Additionally, a part of a random Robinson tiling inflated by a factor τ is superposed to the electron density map. The black dots on its vertices mark positions of possible decagonal ring contrasts on corresponding HRTEM images (cf Beeli *et al* 1991, Hiraga *et al* 1991). All coordinates are given on the v basis.

configuration of the clusters can be derived from the average structure only because of the self-similarity properties of their structures and the strictly limited packing possibilities leading to rather perfect coincidence site lattices, with only a few ambiguities in atomic positions and some more in chemical ordering.

From basic similarities of the electron diffraction patterns of decagonal $Al_{70.5}Mn_{16.5}Pd_{13}$ to those of orthorhombic Al_3Mn, Hiraga and co-workers (1993) concluded a close resemblance of their local structures. This is confirmed, at least for the projected structures, by the great similarity of the respective patterson maps (figure 9 of this work and figure 4 of Hiraga *et al* 1993). Other approximants for this type of decagonal phase are monoclinic $Al_{13}Fe_4$ as was previously demonstrated for isotypic decagonal $Al_{78}Mn_{22}$ (Steurer 1991), and hexagonal μ-$Al_{4.12}Mn$ (Shoemaker 1993). In all the approximant structures pentagonal and decagonal structure motifs can be found in a non-optimum way of packing, i.e. the

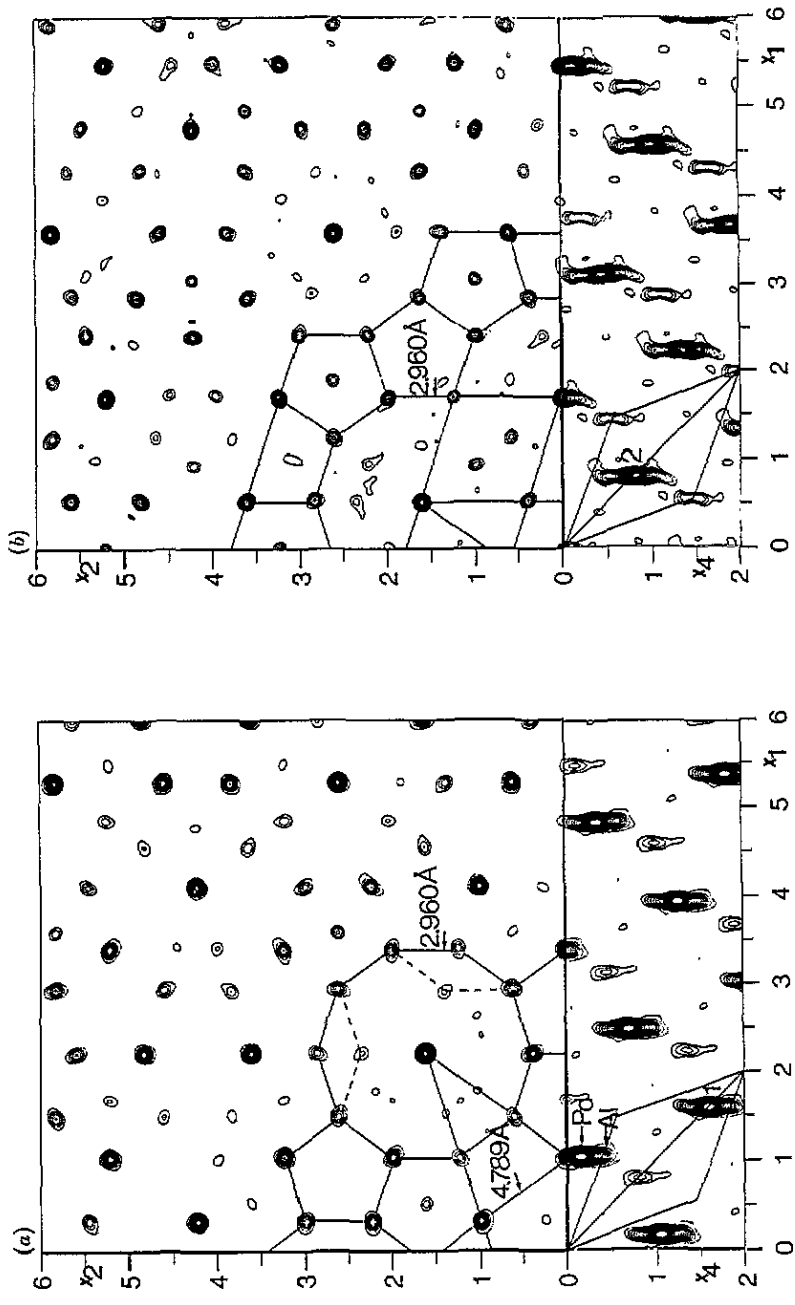
(a)
(b)
2.960Å
4.789Å
Pd
Al
x1
x2
x4

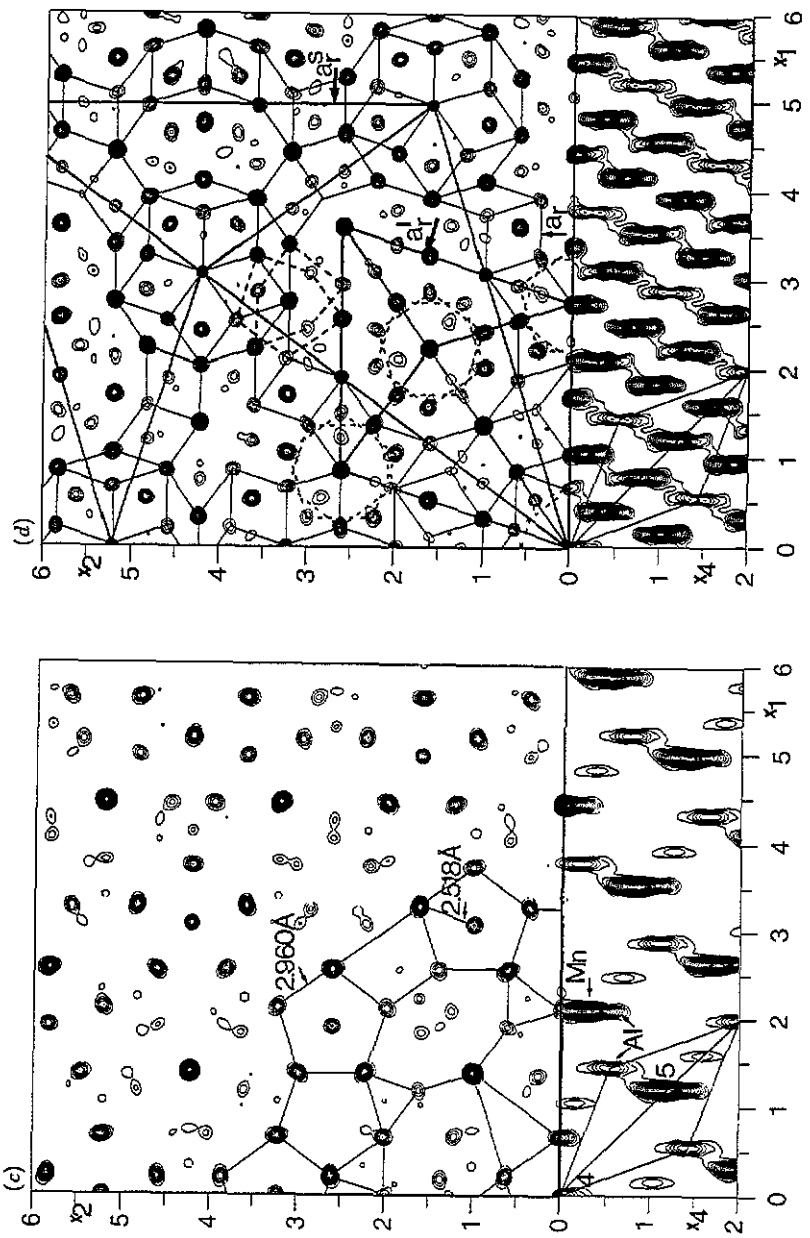

Figure 8. 23.4 × 23.4 Å^2 parallel-space (11000) sections of the 5D Fourier function at (*a*) $x_3 = 0.063$, (*b*) $x_3 = 0.113$, (*c*) $x_3 = \frac{1}{4}$ and (*d*) the projected structure. Additionally, *motifs corresponding to sections of the basic columnar cluster are drawn in.* Projected pentagonal antiprisms in (*d*) are outlined with dotted lines. Penrose and Robinson unit tiles with edge lengths $a_r = 2.518$ Å, $a_r^s = 2a_r(3\sin 2\pi/5 + 2\sin 2\pi/10) = L = 20.29$ Å and $a_r^l = (2\tau + 1)a_r = 10.67$ Å are indicated. Split positions exemplarily marked by dotted lines in (*a*) correspond to those marked in figure 11(*a*) by arrows. The densities in (*a*) and (*c*) are on the same scale; that of (*b*) was multiplied by a factor of three. Thus, (*b*) consists (*mainly*) of Al atoms, (*a*) of Pd and Al and (*c*) of Mn(Pd) and Al atoms. All coordinates are given on the v basis.

eigensymmetry of the structure motifs does not agree with the lattice symmetry. By contrast, quasiperiodicity allows a much more effective packing, without the need to distort these structure elements. It should be emphasized that the term 'approximant' does not necessarily mean that the approximant structure and the decagonal structure are related by a particular 5D rotation; this case would be called 'rational approximant'. It is rather used here in the meaning of 'related structure'.

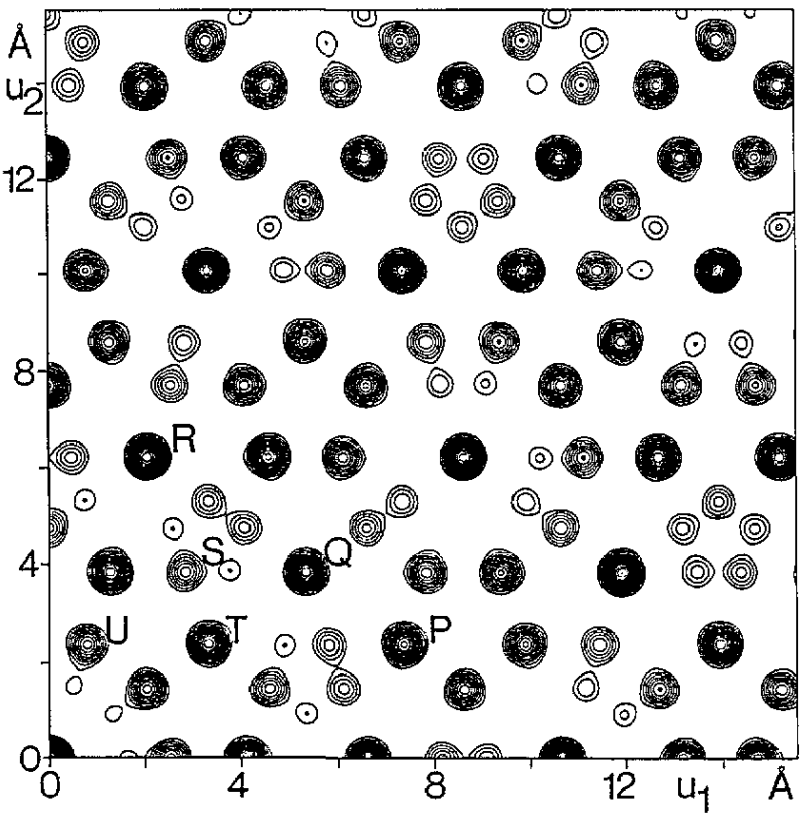

Figure 9. 15.6 × 15.6 Å^2 parallel-space (11000) projection of the Patterson function. Several maxima are marked with letters P–U for comparison with the respective Patterson map of orthorhombic Al_3Mn.

Decagonal $Al_{70.5}Mn_{16.5}Pd_{13}$ is perfectly ordered along the periodic direction (there is no diffuse scattering perpendicular to the layers) while for isotypic metastable decagonal $Al_{78}Mn_{22}$ a doubling of the period is indicated by diffuse interlayer lines on the diffraction patterns. Similar phenomena are observed for decagonal $Al_{70}Co_{15}Ni_{15}$ and $Al_{65}Co_{15}Cu_{20}$ (Frey and Steurer 1993).

4.2. The columnar clusters

From the electron-density maps (figure 8) the cross-sections of the elementary columnar clusters and their linking principles can be derived. The structure motifs found in these sections are dominated by interconnected pentagons, trapezoids and decagons, which form a decoration of an underlying Penrose quasilattice (basic quasilattice) with edge length of the

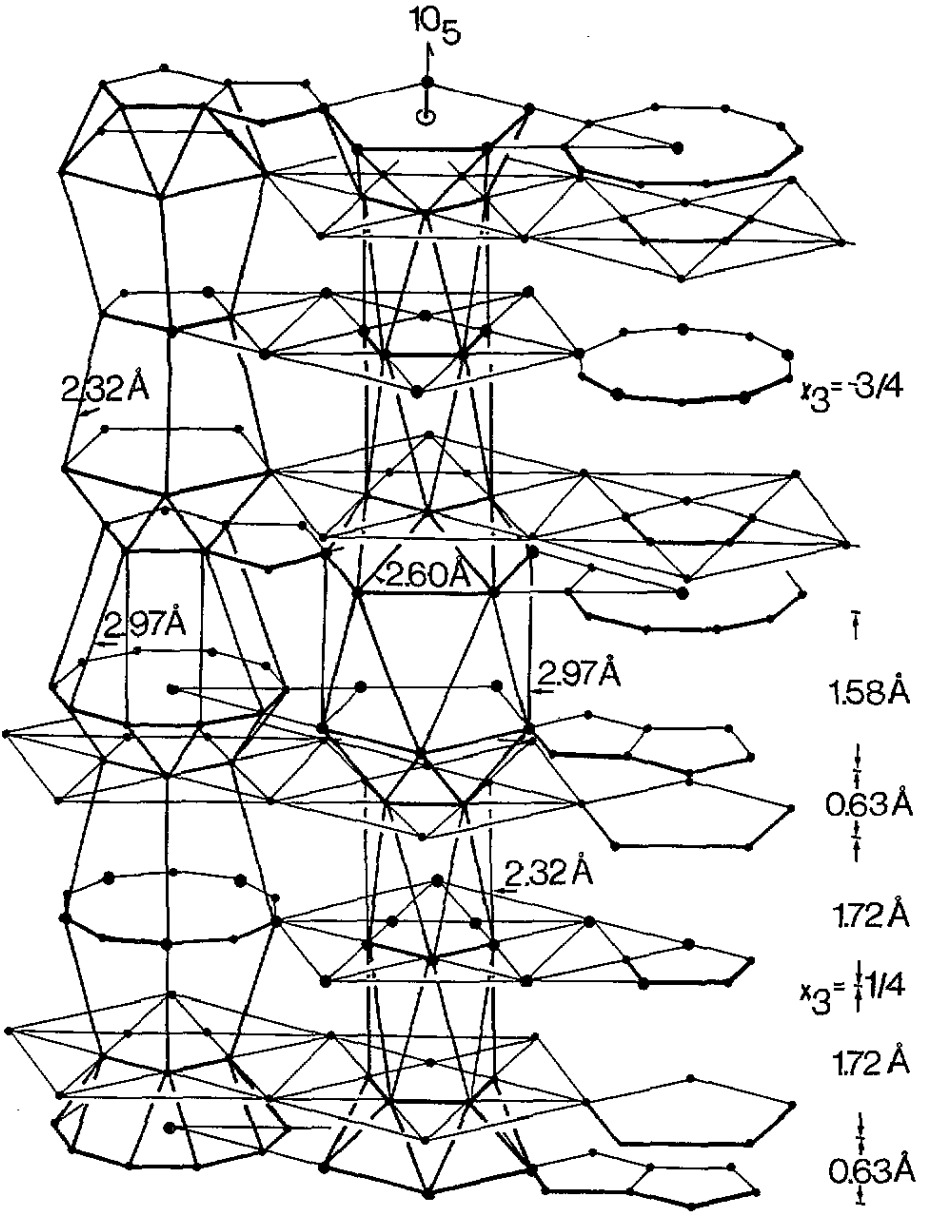

Figure 10. Schematic representation of the layer-stacking principles of a columnar cluster of decagonal $Al_{70.5}Mn_{16.5}Pd_{13}$ along one translation period. Characteristic coordination polyhedra are outlined and typical interlayer distances are given.

unit rhombus $a_r = 2.518(1)$ Å. The electron-density maps also allow a partial reconstruction of the Al/Mn/Pd distribution. The split maxima among others reflect the different ways of atomic relaxation during the coalescence of several columnar clusters.

The in-plane atomic distances, with 2.518(1) Å (radius of a small pentagon) and 2.961(1) Å (edge length of a small pentagon) are significantly larger than the shortest inter-

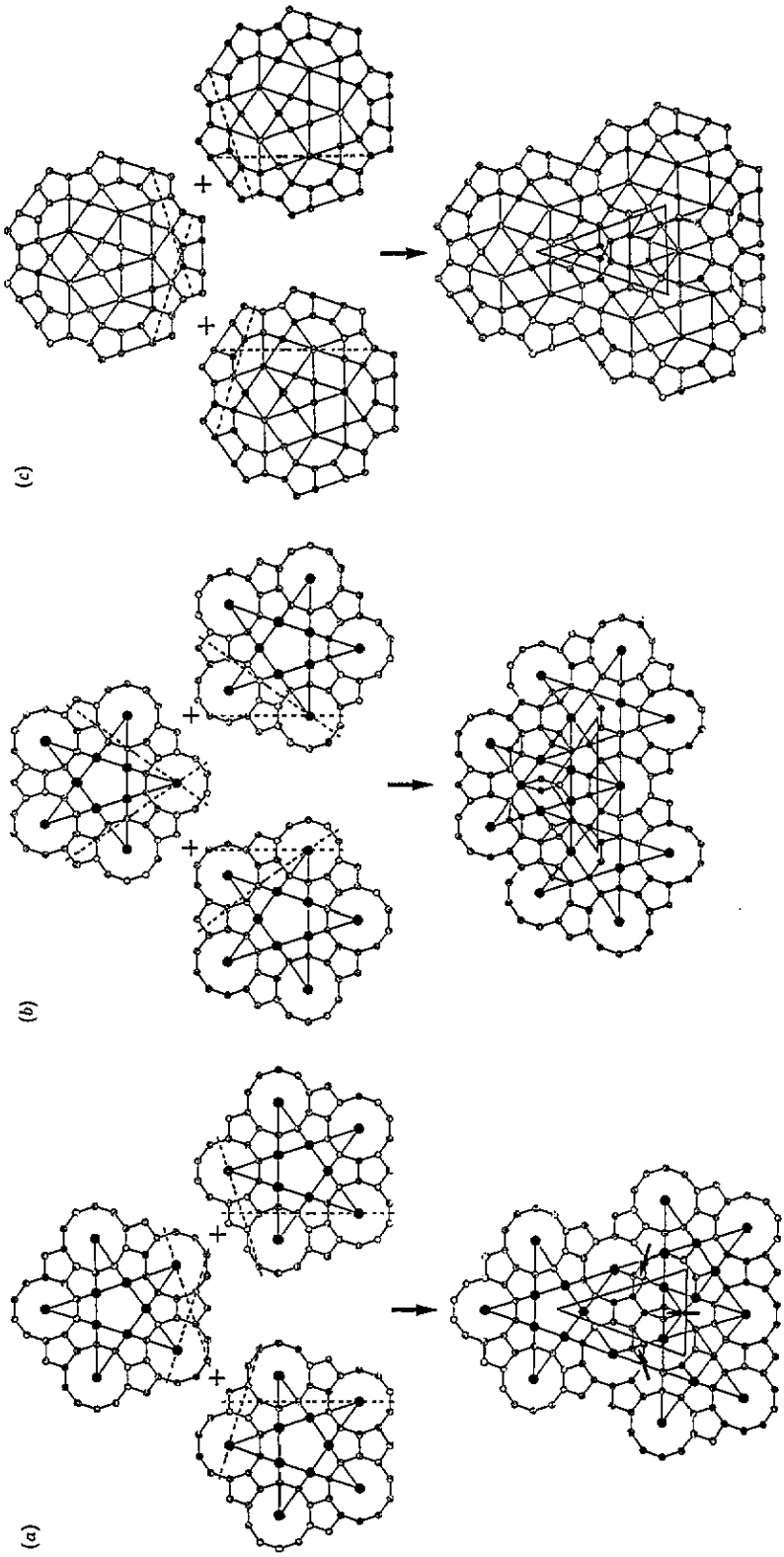
(c)
(b)
(a)

Figure 11. Schematic scenario of the clustering process. The linking of three columnar clusters to large and small Robinson triangles with edge lengths $a_t^s = L$ and $S = L\tau$ are shown for the sections (*a*) and (*b*) in $x_3 = 0.063$, (*c*) and (*d*) in $x_3 = 0.113$, (*e*) and (*f*) in $x_3 = \frac{1}{4}$. Coincidence lines, i.e. mirror lines for the coincidence regions, are drawn with dotted lines. Typical pairs of split positions as occurring in all sections are marked by arrows in (*a*).

planar atomic bond lengths of 2.32 Å, for instance, for the small pentagonal antiprisms (figure 10). Typical bond lengths in intermetallic compounds of similar composition are, for comparison: d_{Al-Al} = 2.60–2.91 Å and 2.527–3.166 Å, d_{Al-Mn} = 2.39–2.80 Å and 2.359–2.874 Å, d_{Mn-Mn} = 2.66–2.78 and 2.678–2.758 Å for orthorhombic Al_3Mn (Hiraga *et al* 1993) and hexagonal μ-$Al_{4.12}Mn$ (Shoemaker *et al* 1989), respectively. The respective Pd distances are slightly larger, such as d_{Al-Pd} = 2.525–2.744(1) Å for tetragonal $Al_{21}Pd_8$ (Range and Christl 1988), and d_{Pd-Pd} = 2.750 Å for elementary Pd. Thus, the small pentagonal antiprisms may preferentially consist of alternating stacked Al and Mn pentagons strongly bonded together. These pentagonal antiprismatic columns running parallel to the columnar cluster axis (one at the centre and ten more around it) appear to be the most stable structure motifs stabilizing the columnar clusters as independent structural units. The structure of such a columnar cluster is shown schematically in figure 10.

Orthorhombic Al_3Mn locally shows a similar stacking sequence along b, the axis being related to the tenfold screw axis of the decagonal phase: antiprismatic pentagonal prisms (a) alternate with pentagonal prisms (p) with the same sequence ... aapaa ... (Hiraga *et al* 1993) as in the peripheral parts of the columnar clusters of the decagonal phase. Hexagonal μ-$Al_{4.12}Mn$ also shows a strong resemblance to the decagonal phase (Shoemaker 1993): the a axis corresponds to a pseudofivefold rotation axis, and many structure motifs occur like the pentagon–trapezoid bands, which are also characteristic of the decagonal phase.

4.3. The packing of the clusters

Starting with one columnar cluster, the coalescence of a second cluster can be carried out with quite perfect coincidence regions in only five symmetrically equivalent orientations and with two different interpenetration depths resulting in centre-to-centre distances L = 20.29(1) Å and $S = L/\tau$ ($\tau = (1+5^{1/2})/2$). For sterical reasons the number of combinations decreases drastically when more clusters are added. In figure 11 the aggregation of, in each case, three clusters into large and small Robinson triangles is shown schematically for different x_3 levels. The coincidence regions contain a few ambiguities in atomic positions (exemplarily marked by arrows in figure 11(a)), which may be separately realized at different sites in the real structure. The ring of ten chains of pentagonal prisms and antiprisms around the centre of a cluster, appearing in the projected structure as small decagons (marked in figure 8(d) by dotted lines) is preserved when two columnar clusters are linked with distance L. For the aggregation of a cluster with distance $S = L/\tau$ these decagonal rings can be presereved only for one cluster; the others become distorted. One such distorted decagon near the centre of a large Penrose rhombus is marked in figure 8(d) by dotted lines. Thus the Robinson triangles become asymmetrically decorated. This explains the observation that in HRTEM images only distances L occur between the decagonal ring contrasts. Parts of the projected electron density mapped in figure 7 were partly superimposed with a random Robinson-triangle tiling, and vertices with distances from each other larger than or equal to L were marked by black dots. Connecting the dots a random Robinson tiling inflated by a factor of τ is obtained. If these inflated Robinson triangles, representing a kind of superstructure of the basic quasilattice of small Penrose rhombi (cf figure 8(d)), are really present in the structure, this has to be reflected in the diffraction pattern: indeed, satellite reflections are observed that can be indexed by wave vectors of length $a_i^{ss*} = 0.124/\tau a_i^* = 0.0766 a_i^*$, $i = 1, \ldots, 4$ (figure 1(a)). A comparison with figures 2 and 4 of the paper by Hiraga and co-workers (1991) confirms that this model is also in agreement with HRTEM images of both the decagonal and nanocrystalline parts of the sample. Without matching rules, these unit tiles combine randomly. Indeed, as indicated by the diffuse scattering, our sample has a high degree of disorder. On the

other hand, the precession photographs indicate that the systematic extinction rules for the Bragg reflections are also valid for the diffuse scattering. This appears to be the crucial point for the interpretation of the diffuse scattering. Since at high temperature no structured diffuse scattering is observed, the structural distortions initiated at lower temperatures must leave invariant the symmetry of the average and the real structure in coherently scattering regions of at least several hundred Å diameter. In the nD description the disorder may then be described by a random fluctuation in phason space, bounded by a periodic wave. The global phason strain is zero because no shifts of reflections could be observed.

The structure model for the columnar clusters of decagonal $Al_{70}Mn_{17}Pd_{13}$ proposed by Hiraga and Sun (1993), considering Al_3Mn as a close approximant of the decagonal phase, has only locally some similarities to the present model. Comparing decagonal Al–Mn–Pd, however, with the structure of icosahedral $Al_{68.7}Mn_{9.6}Pd_{21.7}$ (Boudard *et al* 1992) shows an almost identical electron-density distribution of the projected structures. This is not very astonishing, since the decagonal phase obeys pseudo-icosahedral diffraction symmetry, indicating that the decagonal phase is a closely related approximant of the icosahedral phase. It was also observed that crystals of the decagonal phase epitaxially grown on grains of the icosahedral phase have their tenfold axes parallel to one of the fivefold axes of the icosahedral phase (Beeli 1992). The atomic layers of the decagonal phase have, at least with regard to the atomic positions, their analogues in the icosahedral phase (cf figure 10 of the paper by Boudard *et al* 1992): the layer in $x_3 = 0.065 \cong z_{A5} = 2.522$ Å, the layer in $x_3 = 0.113 \cong z_{A5} = 0.482$ Å, the layer in $x_3 = \frac{1}{4} \cong$ the layer in $z_{A5} = 0.482$ Å, rotated around $2\pi/10$. The decoration with atomic species appears to be different, a natural consequence of the different chemical compositions of the decagonal and the icosahedral phase (Pd is partly substituted for Al compared to the decagonal phase).

5. Concluding remarks

The structure of decagonal $Al_{70.5}Mn_{16.5}Pd_{13}$ can be described as a kind of random tiling of Robinson triangles, with edge lengths $L = 20.29(1)$ Å and $S = L/\tau$. The unit tiles are decorated with columnar clusters, with intracolumnar bonds shorter than intercolumnar ones. The structure of the columnar clusters, on the other hand, corresponds to a decorated Penrose tiling, with edge length of the unit rhombus $a_r = 2.518(1)$ Å. Thus, the structure of the decagonal phase resembles a random tiling of small pieces of an ordered decorated Penrose tiling. The local structure of the decagonal phase shows close resemblance to the local structures of icosahedral $Al_{68.7}Mn_{9.6}Pd_{21.7}$ and of the approximant phases Al_3Mn, μ-$Al_{4.12}Mn$ and $Al_{13}Fe_4$.

Acknowledgment

This work was supported by DFG Ste581/1-2.

References

Beeli C 1992 *Thesis* (Dissertation ETH No 9801) Swiss Federal Institute of Technology, Zurich
Beeli C and Nissen H-U 1993 *J. Non-Cryst. Solids* **153/154** 463–7
Beeli C, Nissen H-U and Robadey J 1991 *Phil. Mag. Lett.* **63** 87–95

Boudard M, de Boissieu M, Janot C, Heger G, Beeli C, Nissen H-U, Vincent H, Ibberson R, Audier M and Dubois J M 1992 *J. Phys.: Condens. Matter* **4** 10 149–68

Frey F and Steurer W 1993 *J. Non-Cryst. Solids* **153/154** 600–5

Henley C L 1991 *Quasicrystals: the State of the Art* ed D P DiVincenzo and P J Steinhardt (Singapore: World Scientific) pp 429–524

Hiraga K, Kaneko M, Matsuo Y and Hashimoto S 1993 *Phil. Mag.* B **67** 193–205

Hiraga K and Sun W 1993 *Phil. Mag. Lett.* **67** 117–23

Hiraga K, Sun W, Lincoln F J, Kaneko M and Matsuo Y 1991 *Japan. J. Appl. Phys.* **30** 2028–34

Ibers J A and Hamilton W C (ed) 1974 *International Tables for X-ray Crystallography* vol IV (Birmingham: Kynoch)

Ma Y, Wang R and Kuo K H 1988 *Scr. Metall.* **22** 1791–6

Okabe T, Furihata J-I, Morishita K and Fujimori H 1992 *Phil. Mag. Lett.* **66** 259–64

Rabson D A, Mermin N D, Rokhsar D S and Wright D C 1991 *Rev. Mod. Phys.* **63** 699–733

Range K J and Christl E G 1988 *J. Less-Common Met.* **136** 277–85

Shoemaker C B 1993 *Phil. Mag.* B **67** 869–81

Shoemaker C B, Keszler D A and Shoemaker D P 1989 *Acta Crystallogr.* B **45** 13–20

Steurer W 1990 *Z. Kristallogr.* **190** 179–234

—— 1991 *J. Phys.: Condens. Matter* **3** 3397–410

—— 1993 *J. Non-Cryst. Solids* **153/154** 92–7

Steurer W, Haibach T, Zhang B, Kek S and Lück R 1993 *Acta Crystallogr.* B **49** 661–75

Steurer W and Mayer J 1989 *Acta Crystallogr.* B **45** 355–9

Tsai A-P, Yokoyama Y, Inoue A and Masumoto T 1991 *J. Mater. Res.* **6** 2646–52

Welberry T R 1989 *J. Appl. Crystallogr.* **22** 308–14

—— 1991 *J. Appl. Crystallogr.* **24** 203–11